JOURNAL OF MATERIALS SCIENCE **36** (2001) 535–546

Adaptive composites incorporating shape memory alloy wires

Part I *Probing the internal stress and temperature distributions with a laser Raman sensor*

G. C. PSARRAS, J. PARTHENIOS, C. GALIOTIS*
Institute of Chemical Engineering and High Temperature Chemical Processes, Foundation for Research and Technology - Hellas (FORTH), P.O. Box 1414, Patras 265 00, Greece
E-mail: c.galiotis@iceht.forth.gr

Hybrid composite laminates consisting of an epoxy resin reinforced by aramid fibres and incorporating SMA wire actuators have been produced. The residual thermal stresses of the composites were determined with the technique of laser Raman spectroscopy and the generated compressive loads during SMA activation were quantified. The results obtained indicate that the SMA wires can be effectively used as actuating elements whereas the aramid fibres can be exploited as independent thermal and mechanical sensors.
© *2001 Kluwer Academic Publishers*

1. Introduction

The selection of materials for a given engineering application is normally based upon their overall physico-mechanical behaviour under static, dynamic and occasional harsh environmental conditions. By combining two or more materials together a much more broader range of properties can be obtained. Nowadays there is a vast population of monolithic or composite materials for the designer to choose from and extensive property-specific tables are available [1]. In many cases, however, an engineering material is required to perform a multitude of functions and this poses an extra difficulty to the selection process. Already, a great deal of research effort is directed in the development of materials that can be classified as "adaptive" or "intelligent". These are materials or material systems certain properties of which, such as stiffness, damping capacity or even shape, may be varied in response to an external or internal stimulus. The mechanism through which such a function is achieved can be "passive" i.e. based solely on the presence of a transformable actuating element or "active" with the integration of actuation and sensing capabilities through an interactive loop [2].

Fibre-reinforced polymeric materials exhibit high intrinsic strength/stiffness per unit weight and excellent fatigue behaviour even in corrosive environments. In addition the current vast choice of constituent materials but also of fibre architecture (e.g. unidirectional tape, 2D and 3D fabrics, etc.) can lead to materials with tailored properties in any given direction. Thus, polymer composites are particularly attractive as candidates for the production of adaptive materials for a number of applications. One special class of adaptive composites is those that incorporate thin shape memory alloys (SMA) in the form of wires, strips or films. In particular, binary Ni-Ti or ternary Ni-Ti-X (where X could be Cu, Co, Fe, or Nb) SMA wires are now commercially available with diameters in the range of 50–200 μm and therefore are ideal for incorporation in fibre reinforced composites. The shape memory effect (SME) that these wires exhibit (Fig. 1) is associated with the reverse transformation from austenite or martensite during cooling or mechanical deformation [3, 4]. In the martensitic phase the boundaries between adjacent martensitic variants can move under the influence of an applied stress resulting in a permanent deformation in the stress direction. Upon heating above a critical temperature the martensite transforms back to the original austenite crystal and the specimen reverts to its original dimensions. After overcoming a temperature hysteresis, the reverse process occurs during cooling (Fig. 1). The whole procedure is governed by two pairs of temperature namely M_s/M_f and A_s/A_f denoting the starting and finishing values of martensitic and austenitic transformation temperatures, respectively. These values are mainly determined by the SMA composition and manufacturing treatment.

The commercial availability of SMA in the form of thin flexible wires of constant diameter and surface condition along its entire length gives them a clear advantage for composite applications over other actuating technologies such as piezolectrics [2, 5]. Other advantages are their high reversible strains (currently up to 10%) and high damping capacity and their ability to generate very high recovery stresses (up to 800 MPa [5]). Among current drawbacks one can mention their

* Author to whom all correspondence should be addressed.

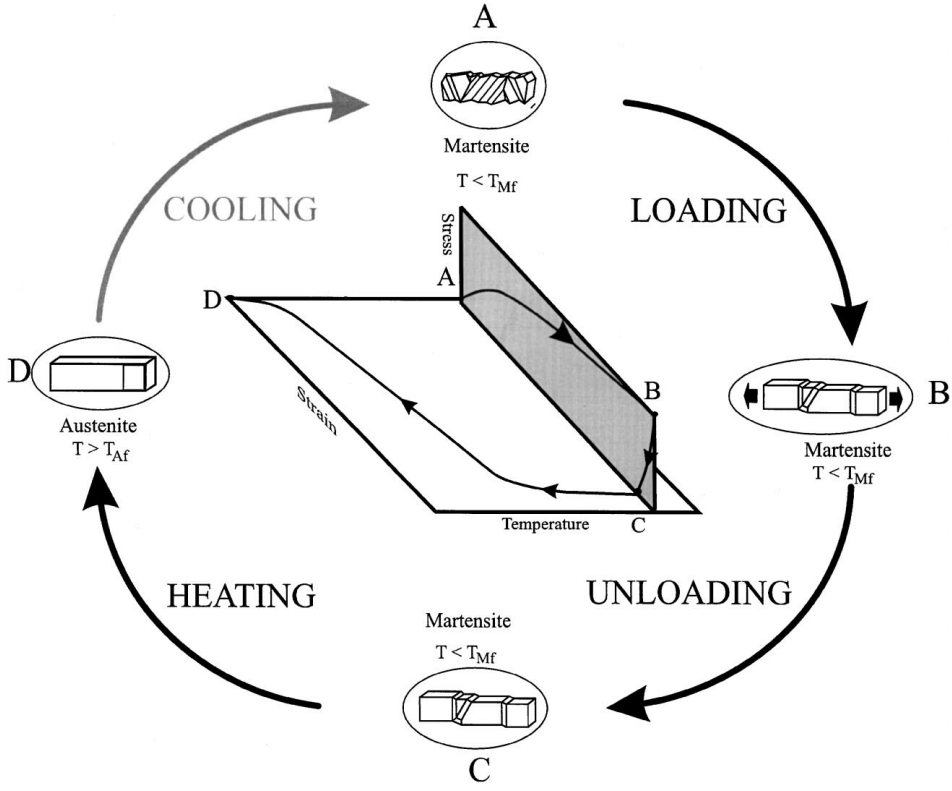

Figure 1 Schematic representation of the Shape Memory Effect. The SMA specimen is deformed (A-B) and unloaded (B-C) at a temperature below T_{Mf}. The resulting plastic deformation is restored during heating to a temperature above T_{Af} (C-D). The original dimensions are re-gained (D-A).

non-linear thermomechanical behaviour and their cooling rate, which can be a limiting factor when high frequency stress/strain input is required in dynamic loading. SMA materials are already exploited in many commercial applications, such as couplings, fasteners, air-conditioning vents, electrical connectors etc. Special mention should be made of their use as biomedical devices, such as dental arches, prosthetic joints, artificial organs etc [6].

The possibility of embedding SMA actuators in the form of a wire or ribbon in a host medium such as a polymeric matrix has been examined by a number of researchers recently [7–13]. The majority of the efforts has been concentrated in developing new engineering materials in which the shape, elastic moduli, internal stress level and natural frequency of vibration can be modified. The emphasis of the potential applications it seems to be on exploiting the high damping capacity of the SMA elements [14] into a "self-controlled" composite structure [15]. Such a "passive" application is based on the enhancement of the vibration damping of the composite material resulting from austenite to martensite transformations below a certain operating temperature [15]. For "active" damping, pre-strained martensitic SMA-wires are embedded into the matrix and when desired they are activated by resistive heating. As a result, recovery stresses are generated and thus the vibration frequency of the material changes [14].

The "active" mode of operation of SMA materials opens a number of opportunities for the development of adaptive materials. Under constrained conditions, the embedded wires operate against the elastic stiffness of the host matrix (pure resin or fibre composite material) biasing their strain recovery. Furthermore, the interface between the wire and the polymer matrix must be sufficiently strong to be able to transmit stresses to the adjacent material. It is therefore of paramount importance to be able to monitor and hence control the generated stresses with a suitable sensor. In this programme of work, the development of adaptive composites consisted of unidirectional aramid fibres (Kevlar 29) embedded in an epoxy resin is investigated. The actuating technology is provided by thin NiTiCu wires, 150 μm in diameter, whereas the technique of laser Raman spectroscopy (LRS) is employed to measure the stress and strain distribution in the aramid fibres during actuation of the SMA wires.

Laser Raman spectroscopy is considered as a powerful method for stress or strain measurements in fibrous composite materials [16]. Past work has shown that Raman vibrational wavenumbers of the skeletal backbone shift to lower values under tension and to higher values under compression and well-defined relationships between Raman wavenumber and applied stress or strain can be obtained for a whole range of polymeric fibres [16–18]. The derived calibration curves have been proved very effective in the determination of fibre stresses or strains in composite materials.

In this paper we report on the first attempts to generate internal stresses in hybrid shape memory alloy wires/aramid fibre/epoxy composites by electrical resistive heating of the wires at different levels of temperature. The incorporation of the actuators into the aramid fibre/epoxy pre-impregnated tapes (prepregs) and the curing methodology is described in detail. A remote laser Raman probe is employed to scan the hybrid composites and to obtain the aramid fibre stress distribution during wire activation. An extra complication

that occurs during laser Raman sampling is the heating up of the aramid fibres during wire activation. Generally speaking, the effect of temperature upon the skeletal vibrations is similar to that of stress i.e. the Raman wavenumber shift is a decreasing linear function of temperature. Therefore, the thermal contribution should be known and subtracted from the total wavenumber shift in order to obtain the stress distribution. Normally, this can be done by independent temperature measurements with a thermocouple and/or an infrared thermal camera. In this work, however, we have employed the Raman wavenumber shift of a non-skeletal vibration, which is insensitive to temperature, to extract the stress values and therefore the temperature distribution was obtained by subtraction from the skeletal wavenumber shift. Thus we have developed a laser Raman spectroscopic (LRS) methodology whereupon the aramid fibres can both act as independent temperature and stress sensors in the composites that they reinforce. The results showed that different levels of thermal activation of the SMA wires, led to different grades of stress/strain recovery within the hybrid composite. The suitability of the SMA wires as actuating elements in polymer composites and the LRS response of the reinforcing aramid fibres as an effective thermal and mechanical sensor is discussed.

2. Experimental

2.1. Materials

In this study Kevlar 29 supplied by Du Pont were used as reinforcing fibres. The choice for these aramid fibres was based on their Young's modulus (∼70 GPa) compatibility with the SMA wires. The diameters of individual Kevlar 29 filaments were measured by employing a laser diffraction unit and their mean value was found to be 15.9 ± 0.5 μm. The LTM217 one-part epoxy resin was supplied by the Advanced Composites Group (ACG). The selection of the resin was based on its suitability for prepreg manufacturing and on its high T_g in order to avoid severe modulus relaxation during resistive heating of the wires.

Unidirectional prepeg tapes of Kevlar 29/LTM217 of 53.5% in fibre volume fraction were also supplied by ACG. The curing procedure involved initial curing at 70° C for 12 h followed by post-curing at 140° C for 1 h. The final T_g for the epoxy system was found to be just above 150°C, which is considered adequate for this application as it is higher than the upper temperature ceiling required for the martensite-austenite transformation.

TABLE I Transformation temperatures of the NiTiCu wire

M_s/°C	M_f/°C	A_s/°C	A_f/°C
46.8	38.3	55.6	64.2

For the preparation of the hybrid composite systems, NiTi(12%)Cu SMA wires, 150 μm in diameter, supplied by Memry Co., were used in different volume fractions and geometries. In Table I the characteristic transformation temperatures are listed. A specially designed mould was used in the production of hybrid composite plates. This mould contained a frame suitable for pre-straining the wires and for maintaining the tensile strain, as well as, for keeping the wires aligned during cure. The inter-wire distance could also be fixed with the same frame. As shown in Fig. 2, the layer of the parallel wires were pre-strained by 3% and were placed between equal number of plies before being incorporated into the autoclave bag. The employed autoclave curing conditions were identical for all the types of specimens. In this study the examined specimens were a plain 4-ply epoxy resin/aramid fibre laminate (abbreviated to O_4^0), a 2-ply specimen incorporating 3 wires in the mid-plane (abbreviated to $O_1^0/W_3/O_1^0$) and a 2-ply specimen incorporating 9 wires in the mid-plane (abbreviated to $O_1^0/W_9/O_1^0$).

2.2. Laser Raman microscopy

Raman spectra were obtained using the 514.5 nm line of an Ar-ion laser as the excitation wavelength. The laser beam was polarised along the fibre axis for all Raman measurements. A modified Nikon microscope was used for focusing the laser beam to a 2 μm spot on the fibre through a suitable objective lens. The 180° backscattered beam was collected by the same microscope objective and focused on the entrance slit

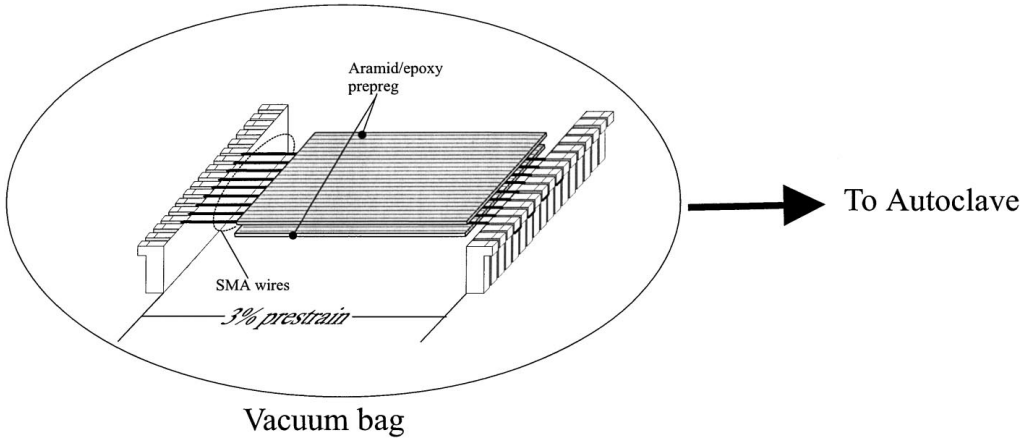

Figure 2 The mould used for the production of hybrid composite plates. This mould contains a frame suitable for aligning the wires and then pre-straining and maintaining the tensile strain (3%) during curing.

of a SPEX 1877 triple monochromator. Finally, the spectrometer dispersed light was directed to a Wright instruments CCD (Charged Couple Device) detector, which was used as a photon detecting system and the Raman spectra were recorded on a PC. The spectral characteristics within the wavenumber range of 1100 to 1800 cm^{-1}, were derived by fitting the raw data of the 1648 cm^{-1} band with a Lorentzian function and that of the 1611 cm^{-1} Raman band with mixed Lorentzian/Gaussian functions.

The acquisition of Raman data used for the determination of the stress calibration curves was performed with a Remote laser Raman Microprobe (ReRaM). The ReRaM has been developed and tested in-house and uses flexible waveguides for both the delivery and the collection of light [16, 19]. Micrometer stages allow the translation of the ReRaM in all three axes down to an accuracy of 1 μm. The use of an incorporated CCTV camera allows optical observations of the specimen during Raman data acquisition. The collected Raman light is guided through an optical fibre to a SPEX 1000 M single monochromator. Finally the collected Raman signal via a Wright Instrument CCD is stored in a PC. This remote setup is particularly useful for composite materials subjected to mechanical loading, but it can, also, be used in a whole variety of technological applications where conventional micro-Raman arrangements impose space restrictions to the actual measurements.

The influence of temperature on the Raman response of the aramid fibres was examined with the usage of a THMS 600 (Linkam Scientific Instruments Ltd) hot stage. This was mounted on the Raman microscope platform and the desired temperature profile was applied by the TMS 93 controller supplied by the same company. The ramp up rate of the profile was 1 °C/min and each ramp was followed by a dwell stage for a sufficient period of time (>5 min) to achieve temperature equilibrium in the fibres. The range of the applied temperature was varying from ambient to 150 °C.

The stress sensitivity of the Raman wavenumber of the Kevlar 29 fibres was obtained by loading the fibres on a Hounsfield H25KM mechanical frame. The relation of applied stress with the recorded Raman shift was investigated by employing a 20 N load cell. The obtained Raman data were fitted to appropriate distribution functions and statistically analysed, as described above.

2.3. SMA activation

The experimental set up used during the SMA wires actuation is schematically depicted in Fig. 3. This set up allows the recording of the Raman spectra during SMA-wire activation and the simultaneous control of the wire temperature. The wires in the hybrid composites are connected in-series and by adjusting the current and, thus, the wire temperature, stress is generated in

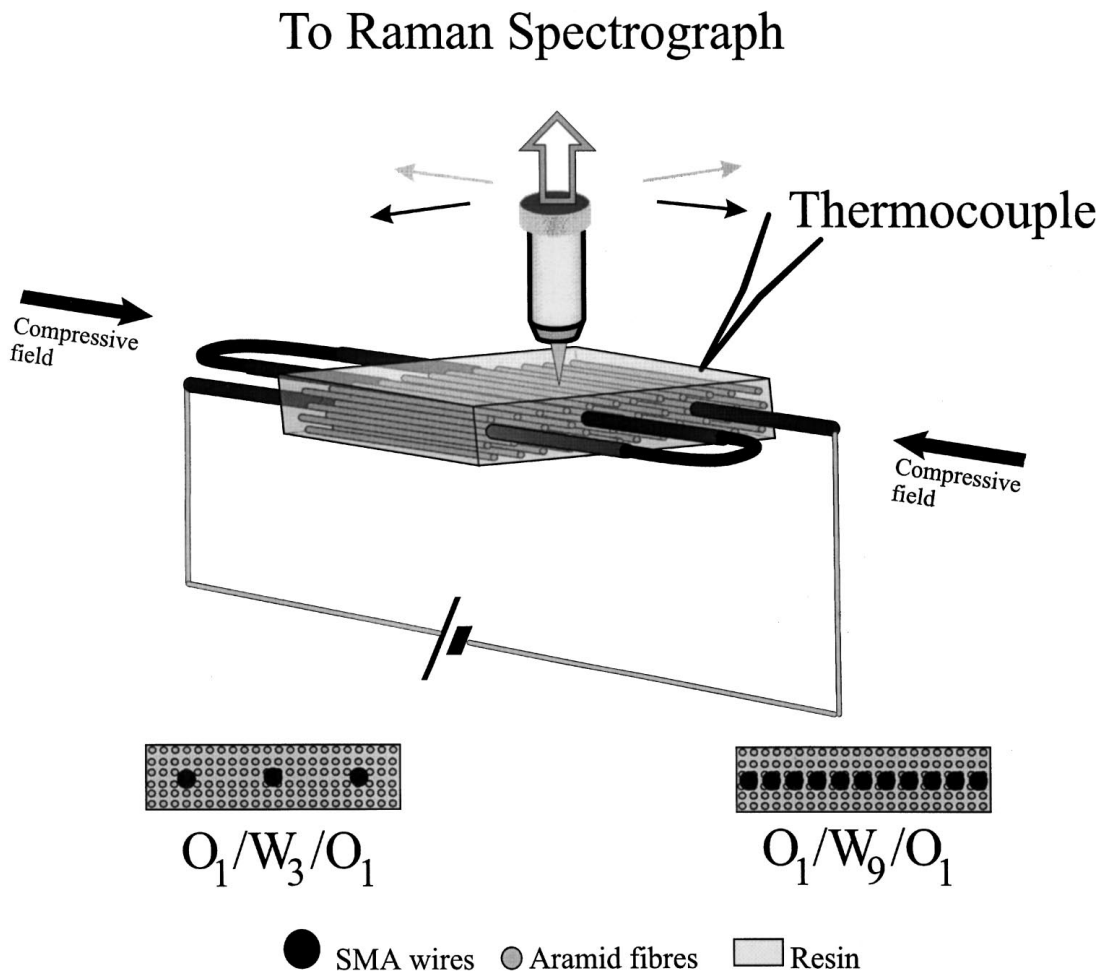

Figure 3 Experimental setup for SMA composites activation. The wires are activated by resistive heating and as result a compressive field is generated. The figure shows two hybrid geometry cross-sections with 3 and 9 wires respectively.

a controlled fashion. The voltage on the wire circuit is applied by an Aplab ZT3203 regulated DC power supply, whereas the electrical current and voltage are measured by a couple of Benning digital multitesters. Finally, temperature measurements were conducted at different points on the surface of the specimen and on a wire outside the specimen by suitable tiny thermocouples (diameter less than 100 μm) supplied by Omega Engineering Inc. The temperature is kept constant during Raman data acquisition aiming to achieve a non varying force field. The hybrid systems were also tested along the same sampling directions by interrupting the resistive heating on the completion of the actuation experiment and after allowing the specimen temperature to return back to ambient.

3. Results

3.1. Aramid fibres as temperature and stress sensors

The micromechanical investigation of the hybrid composites is based on monitoring the deformation of two specific vibrations of the polymer backbone. These vibrations recorded at 1611 and 1648 cm^{-1} (Fig. 4) correspond mainly to ring/C-C stretching and to amide/C=O stretching respectively [20]. Both bands have been proved stress sensitive and calibration curves have been derived by recording the peak position of the bands with respect to an applied mechanical stress (Fig. 5a and b). Both set of results were least-squares-fitted with straight lines of slope of -4.1 ± 0.4 cm^{-1}/GPa and -2.0 ± 0.4 cm^{-1}/GPa for the 1611 cm^{-1} (Fig. 5a) and 1648 cm^{-1} (Fig. 5b) vibrations, respectively.

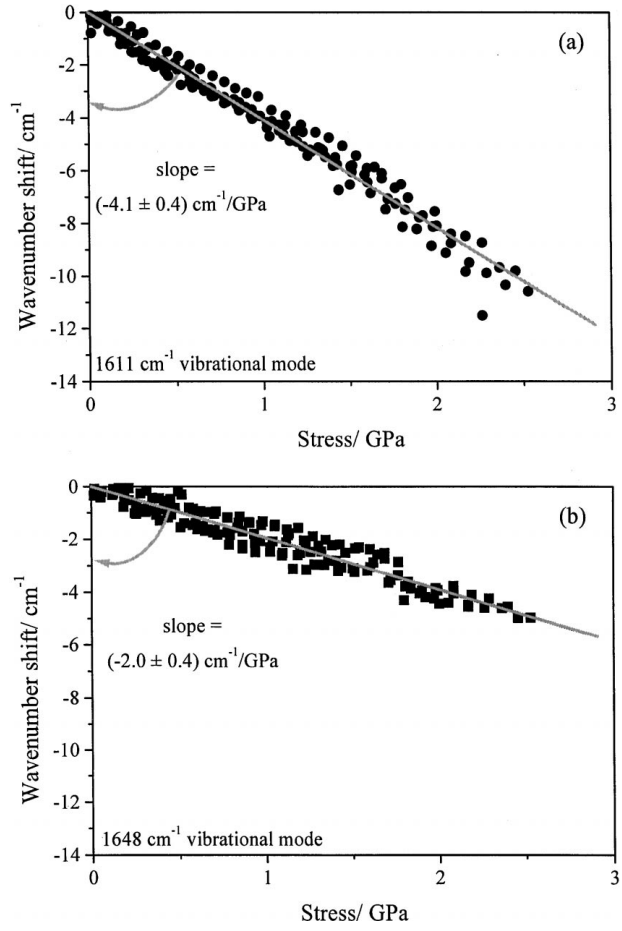

Figure 5 Raman wavenumber shift as a function of the applied stress for the Kevlar 29 fibres, (a) 1611 cm^{-1} Raman band and (b) 1648 cm^{-1} Raman band. The data points present results from 5 different experiments.

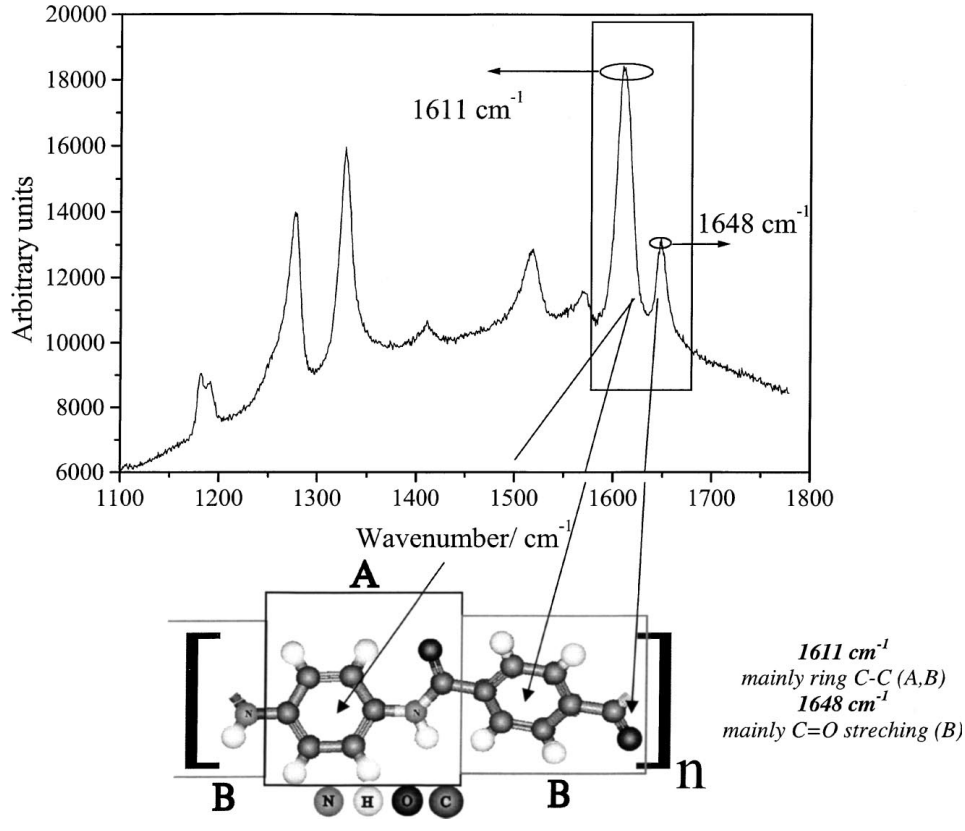

Figure 4 Aramid fibre Raman spectrum in air, indicating the nature of the two vibrational modes used in the present study.

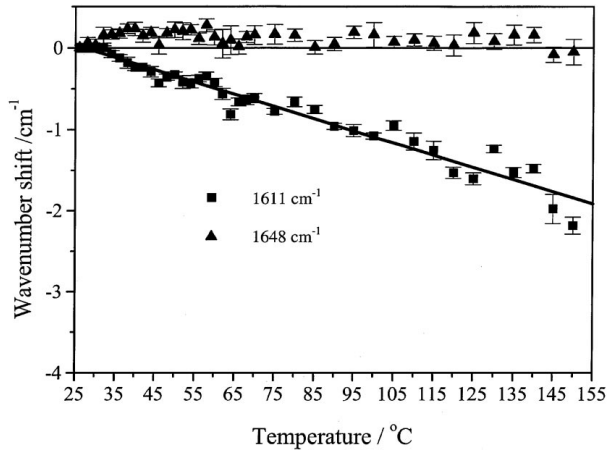

Figure 6 Raman wavenumber shift as a function of temperature. Each experimental point represents an average of 10 measurements.

The influence of temperature was determined by monitoring the induced changes in the vibration peak wavenumber by the applied thermal field. The results of this investigation are depicted in Fig. 6 and it is clear that the position of the 1611 cm^{-1} band depends on the fibre temperature while the 1648 cm^{-1} equivalent can be considered as temperature insensitive. The Raman wavenumber shift of the 1611 cm^{-1} band is least-squares-fitted with a straight line of slope of (-0.015 ± 0.001) cm^{-1}/°C (Fig. 6).

3.2. Determination of residual thermal stresses

During the manufacturing process of the composites residual thermal stresses are developed as a result of the mismatch of the thermal expansion coefficients of the fibres and the matrix [21]. In the case of aramid/epoxy composites the fibres are subjected to residual compression whereas the matrix is in tension. It is worth adding here that the existence of pre-strained wires could influence the residual thermal stress distribution. Thus, an accurate estimation of the residual stresses is a prerequisite for the determination of the stress distribution in the hybrid composites during and after the activation of the SMA wires.

LRS measurements combined with a suitable statistical analysis can provide accurate values for the residual stresses [22]. Raman sampling is performed along two direction normal and parallel to the fibre axis and at steps of approximately one fibre diameter. The Raman wavenumber distribution of the free-standing fibres in air is obtained by collecting 100 Raman spectra from random positions within a batch of fibres just prior and just after each experiment. Since the errors encountered at this stage are non-biased, the results are normally expressed with a Gaussian function [21, 22]. The same procedure is repeated for the embedded fibres and the results are also fitted at a first approximation with Gaussian functions.

The Gaussian (normal) frequency distribution function $y(x)$ can be expressed by [23]:

$$y(x) = \frac{Ne^{-(x-\mu)^2/2s^2}}{s\sqrt{2\pi}} \qquad (1)$$

where N is the number of measurements, μ is the arithmetic mean value and s the standard deviation. Equation 1 can be transformed to a normalised Gaussian distribution function [23] where the probability (density) function $P(x)$ is written as:

$$P(x) = \frac{e^{-(x-\mu)^2/2s^2}}{s\sqrt{2\pi}} \qquad (2)$$

It is evident that the sum of all probabilities is equal to unity and hence the area enclosed by the curve of Equation 2 should also be equal to one. The obtained distribution functions are represented in Figs 7a, 8a and c, and 9a. In order to derive the net Raman wavenumber shift due to curing and post-curing process the resulting distributions of fibres in air and of fibres embedded in the composite must be statistically subtracted [22]. The probability density function of the difference of two sets of measurements described by Gausssian distributions is given by [23]:

$$P(z) = \frac{e^{-[z-\mu]^2/2\left(s_1^2+s_2^2\right)}}{\sqrt{2\pi\left(s_1^2+s_2^2\right)^{1/2}}} \qquad (3)$$

where $z = x_2 - x_1$ is the difference of the two variables, $\mu = \bar{x}_2 - \bar{x}_1$ the difference of the corresponding

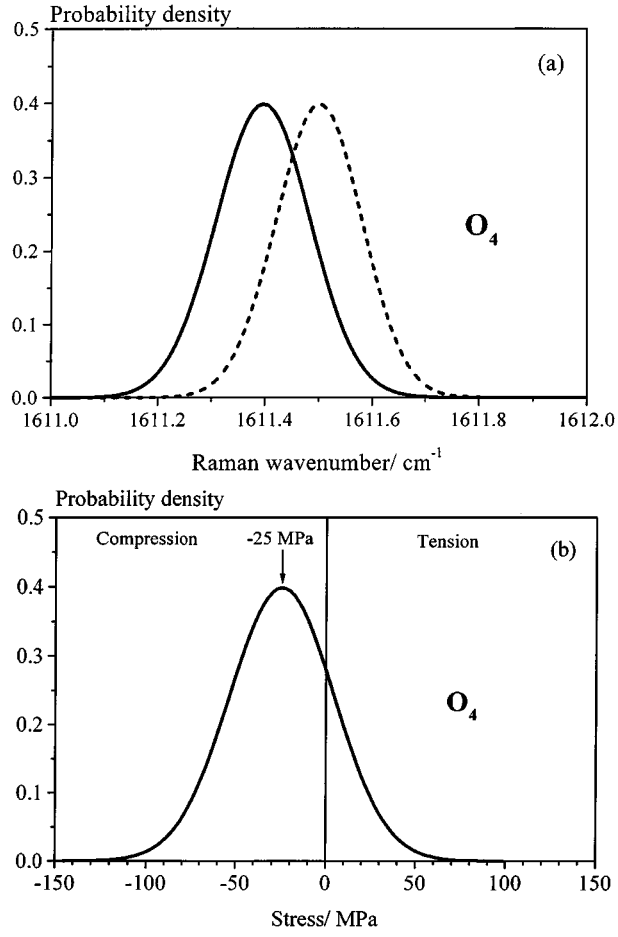

Figure 7 Gaussian frequency distributions of (a) Raman wavenumber shift of free-standing Kevlar 29 fibres (dashed line) and from fibres embedded in the O_4^0 specimen (solid line); (b) the corresponding residual thermal stress distribution. The mean value of the distribution is −25 MPa.

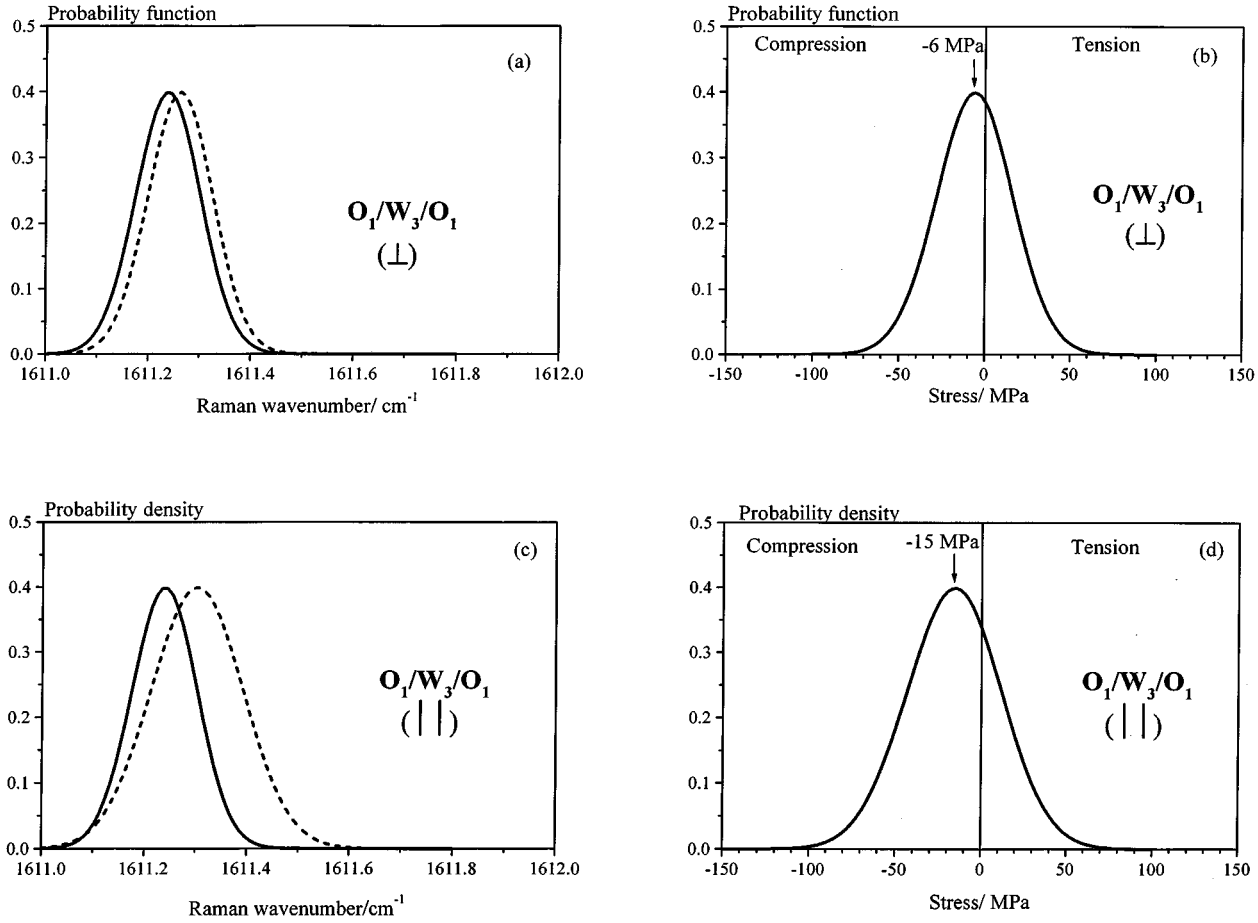

Figure 8 Gaussian frequency distributions from spectra taken from the $O_1^0/W_3/O_1^0$ specimen. (a) Raman wavenumber shift of free-standing Kevlar 29 fibres (dashed line) and from fibres embedded in the hybrid composite (solid line) along a line normal to the wire direction. (b) The corresponding residual thermal stress distribution. (c) Raman wavenumber shift of free-standing Kevlar 29 fibres (dashed line) and from fibres embedded in the hybrid composite (solid line) along a line parallel to the wire direction. (d) The corresponding residual thermal stress distribution.

arithmetic means with $\bar{x}_1$ being the smaller value and s_1, s_2 the standard deviations of the initial distributions. In the final step the resulting Raman shift distribution is converted into stress through the predetermined Raman wavenumber calibration factor.

Detailed LRS mapping of the free-standing samples has been performed at some distance from the coupon ends in order to avoid the influence of the specimen ends. The number of measurements N, the standard deviation s, and the mean value μ, of all the systems examined and the corresponding free-standing fibres are listed in Table II. The determined stress distribution of the examined samples are presented in Figs 7b, 8b and d, and 9b. In all cases, the average values of thermal residual stresses are considered as reasonable for the curing/post-curing cycle employed in this work.

TABLE II Statistical parameters used/evaluated during the determination of the residual thermal stresses in the composites and the corresponding volume fraction of SMA wires in the examined samples

	N	s/cm^{-1}	μ/cm^{-1}	vol. fraction of SMA/%
O_4^0	200	0.08	1611.50	0
Free standing aramid fibres	200	0.09	1611.40	—
$O_1^0/W_3/O_1^0$ parallel to the wires	100	0.14	1611.30	1.0
$O_1^0/W_3/O_1^0$ normal to the wires	163	0.12	1611.26	1.0
Free standing aramid fibres	200	0.08	1611.24	—
$O_1^0/W_9/O_1^0$ normal to the wires	220	0.09	1611.26	3.5
Free standing aramid fibres	200	0.06	1611.20	—

3.3. Stress distribution during SMA activation

For every stage of the applied temperature the prestrained wires are generating a different level of compressive stress. The development of the compressive field inside the composites is influencing the Raman wavenumber shift of the aramid fibres by increasing the vibration wavenumber of the recorded bands. On the other hand, the generated heat by the wires is slowly dissipated in the composite and thus is affecting the Raman wavenumber shift of the fibres by decreasing the vibration wavenumber of the 1611 cm^{-1} band as shown in Fig. 6. For every level of activation the Raman response of the fibres normal and parallel to the wire direction was obtained (Figs 10 and 11). Since only a part of the recorded Raman wavenumber shift corresponds to

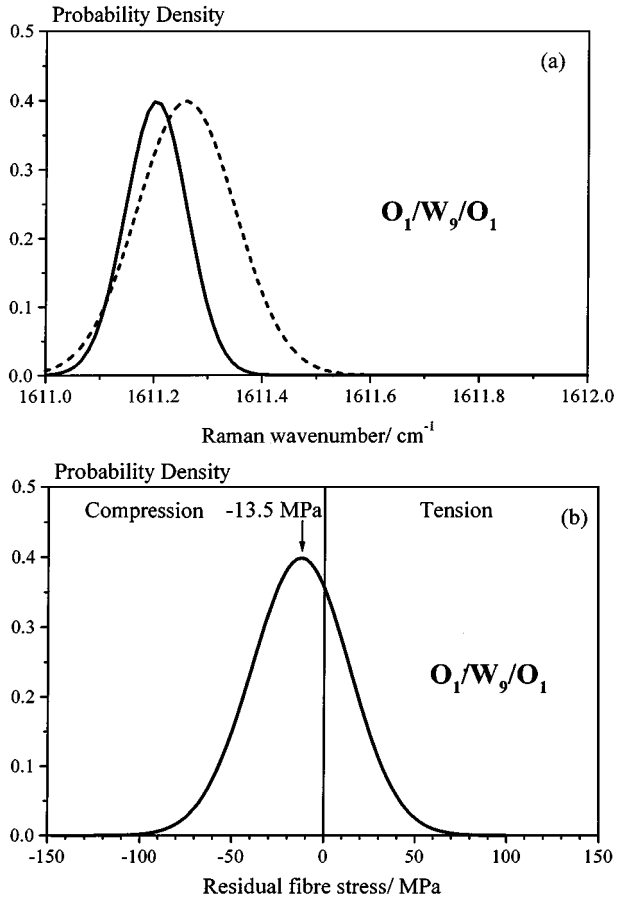

Figure 9 Gaussian frequency distributions of (a) Raman wavenumber shift of free-standing Kevlar 29 fibres (dashed line) and from fibres embedded in the $O_1^0/W_9/O_1^0$ specimen (solid line); (b) the corresponding residual thermal stress distribution. The mean value of the distribution is −13.5 MPa.

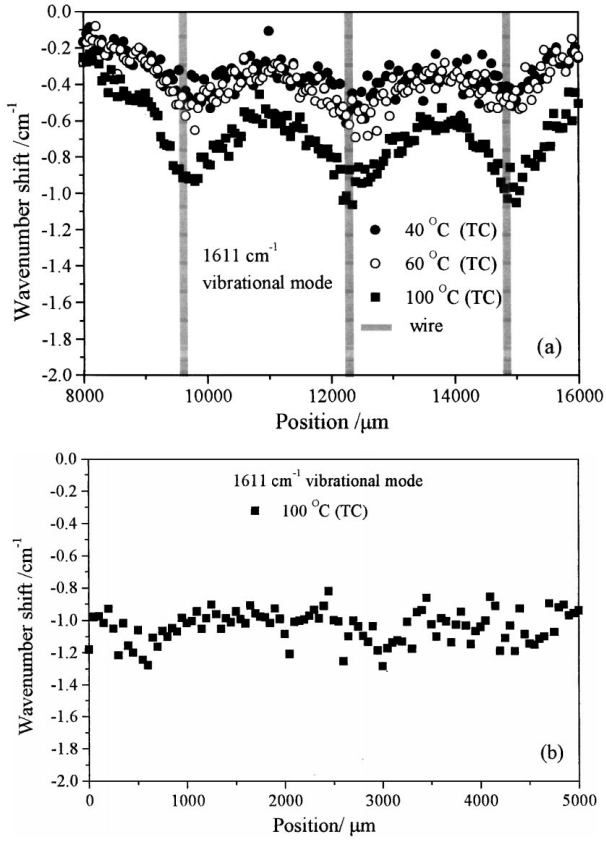

Figure 10 Total Raman wavenumber shift due to the 1611 cm^{-1} band of the $O_1^0/W_3/O_1^0$ specimen. (a) Across the wire direction for different levels of activation. The solid vertical lines depict the location of the SMA wires. (b) Along the wire direction at 100 °C.

the induced mechanical load from the activated wires it is necessary to develop a methodology capable to distinguish the contributions of all acting parameters. After eliminating the contributions of temperature and residual stress, the recorded shifts can be converted to stresses using the universal Equation [18]:

$$\Delta\nu_M = k\sigma \tag{4}$$

where k is the Raman wavenumber shift coefficient with stress for a given Raman band.

In the case of the $O_1^0/W_9/O_1^0$ specimen the generated stresses caused the geometrical failure of the specimen in compression. As shown in Fig. 12 at activation temperatures as high as 130°C the induced compression brings about the warping of the whole composite coupon. Thus, successive areas where the fibres were subjected to tensile load ("peaks") alternate with areas where the fibres are in compression ("troughs"). In Fig. 13 the gradual increase of the amplitude of the buckling deformation along a representative length, L, of the coupon is shown for activation temperatures of 35, 60, 92 and 120 °C. It is interesting to note that if the activation temperature exceeds 100°C then a permanent buckling deformation is observed when the material is cooled down to ambient temperature. The stresses experienced by the aramid fibres when the laminate is at the "warped" state at ambient temperature can easily be measured by LRS employing the highly stress-sensitive 1611 cm^{-1} band through Equation 4. The results for a section of the laminate that shows a single buckling wave ("peak" to "trough") are shown in Fig. 14. As expected the fibre stresses are tensile on the protruded "peak" of maximum 250 MPa and compressive of about −150 MPa along the inner "trough". A final observation is that the permanent deformation gradually diminishes as the wires overcome the temperature hysteresis and revert back to their maternsitic state.

4. Discussion

4.1. Residual thermal stresses

The residual thermal stresses play an important role in the overall performance and lifetime of fibrous polymeric materials. The manufacturing process of composite materials often employs high curing and/or post-curing temperatures which give rise to the development of residual thermal stresses upon cooling and solidification. Their development is attributed to the mismatch between the thermal expansion coefficients of the fibre and the matrix. A great deal of work has been done already on carbon fibre based systems [20–22, 24] but little work has been carried out on aramid fibre composites [13, 25].

Comparing the normalised Gaussian distribution of the Raman response of free-standing aramid fibres with that obtained from the embedded Kevlar fibres (Figs 7–9), it becomes apparent that the 1611 cm^{-1}

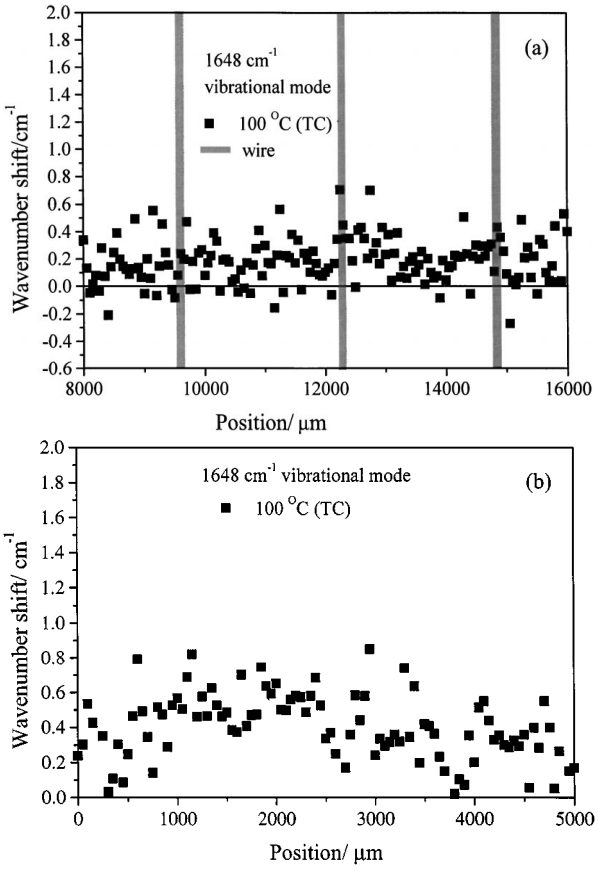

Figure 11 Total Raman wavenumber shift due to the 1648 cm^{-1} band of the $O_1^0/W_3/O_1^0$ specimen at 100 °C. (a) Across the wire direction. The solid vertical lines depict the location of the SMA wires and (b) along the wire direction.

wavenumber band of the latter shifts to higher values. This behaviour is common in both the epoxy resin/Kevlar 29 fibres system and in the hybrid systems and implies that the aramid fibres in the composites are subjected to compression as a result of the curing/post-curing procedure. The derived mean values of the thermal stresses for the O_4^0, the $O_1^0/W_3/O_1^0$ and the $O_1^0/W_9/O_1^0$ systems along a line vertical to the wire direction (Figs 7b, 8b, and 9b) are −25 MPa, −6 MPa and −13.5 MPa respectively. These values are relatively low in magnitude and can be attributed to the slow heating rate employed (0.33 °C/min) during curing and post-curing. Furthermore, the mean value of the residual compressive stress appears to broadly decrease as the wire volume fraction increases. This result appears to be a direct consequence of the stresses developing during curing; since the wires are prevented from contracting (martensite-austenite transformation) as a result of the imposed 3% pre-strain (see tensile frame, Fig. 2), tensile stresses are developing during curing which are transmitted to the neighbouring fibres. The net effect is a reduction of the residual compressive stresses than the fibres would have if the constrained wires were not present.

4.2. Real-time temperature and stress measurements in SMA composites

The total Raman wavenumber shift during SMA activation in the $O_1^0/W_3/O_1^0$ system in directions parallel and perpendicular to the wire axis is presented in Figs 10a and b and 11a and b for the 1611 cm^{-1} and 1648 cm^{-1} bands, respectively. The wavenumber shift depicted is given by:

$$\Delta\nu = \Delta\nu_M + \Delta\nu_\theta + \Delta\nu_R \quad (7)$$

where $\Delta\nu_M$, $\Delta\nu_\theta$ and $\Delta\nu_R$ are the contributions of "activation" stress, temperature and residual stress in the Raman wavenumber shift, respectively. In the case examined here, the term $\Delta\nu_M$ is positive for both Raman bands since the applied force field is compressive. The term $\Delta\nu_\theta$ is varying linearly with temperature remaining always negative for the 1611 cm^{-1} band, whereas it assumes a constant positive value for the 1648 cm^{-1} band (Fig. 6). Finally the $\Delta\nu_R$ term can be measured separately prior to wire activation as described previously.

4.2.1. $O_1^0/W_3/O_1^0$ specimen

4.2.1.1. Stress measurements during wire activation. For the 1648 cm^{-1} Raman band, the vibrational wavenumber exhibits an average constant increase $C = 0.117$ cm^{-1} within the 30–150°C temperature range (Fig. 6):

$$\Delta\nu_{\theta,1648} = C \quad (8)$$

The Raman wavenumber shift as a function of stress, $\Delta\nu_{M,1648}$, can be described by the following linear relationship:

$$\Delta\nu_{M,1648} = k_{1648}\sigma \quad (9)$$

where the slope $k_{1648} = -2.0 \pm 0.4$ cm^{-1}/GPa is assumed to be constant at any given operating temperature.

By rearranging Equations 7–9 the axial stress transmitted to the fibres by wire activation as determined by the 1648 cm^{-1} band is given by:

$$\sigma = \frac{\Delta\nu_{1648} - \Delta\nu_{R,1648} - C}{k_{1648}} \quad (10)$$

where $\Delta\nu_{1648}$ is the total wavenumber shift and $\Delta\nu_{R,1648}$ is the wavenumber shift due to the residual stress. The resulting stresses across and along the wire direction for an activation temperature of 100°C for the $O_1^0/W_3/O_1^0$ specimen are given in Fig. 15a and b. As can be seen, most fibre measurements indicate compression stresses of average 90 MPa. There is a tendency for the peaks of the stress distribution to "cluster" around the plane of the wires themselves. The high scatter of the data points is attributed to the low sensitivity of the 1648 cm^{-1} stress sensor and some real variations in the material since for such a low volume fraction of wires, the stress is not expected to be uniform across the wire direction (Fig. 15a). The results collected along the middle wire are less scattered and the average value obtained of 122 MPa is higher than that measured in the normal direction due to the proximity in this case of the interrogated fibres to the activated SMA wire. Finally, it is worth reiterating that through Equation 10 the stress is measured point by point in the fibre and at a spatial resolution as small as 1 μm.

4.2.1.2. Temperature measurements during wire activation. As mentioned earlier the 1611 cm^{-1}, the Raman band is sensitive to both stress and temperature (Figs 5a

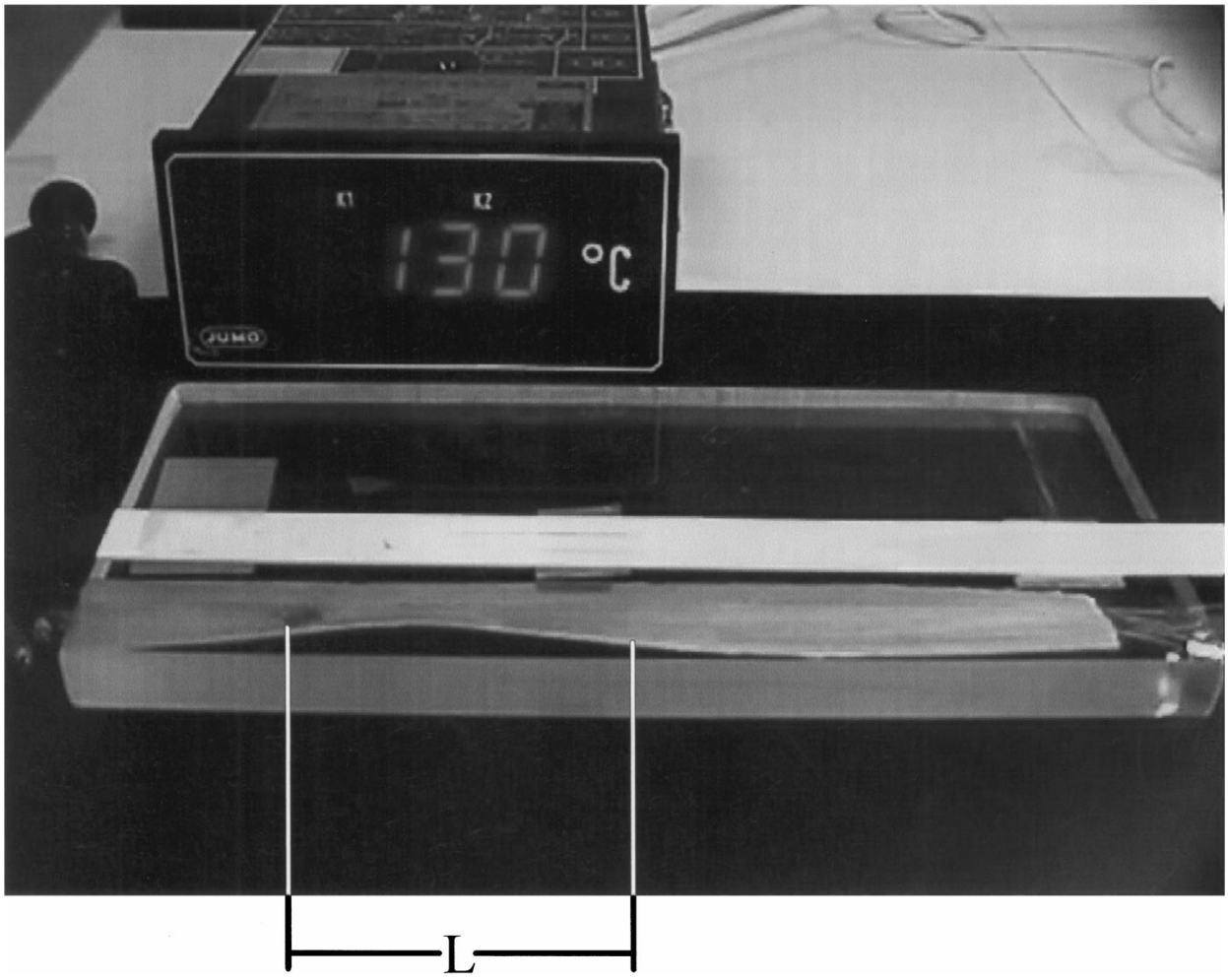

Figure 12 Experimental set up showing wire activation at a temperature of 130°C for the $O_1^0/W_9/O_1^0$ specimen. The composite coupon has visibly buckled at that level of activation. The indicated length $L = 50$ mm.

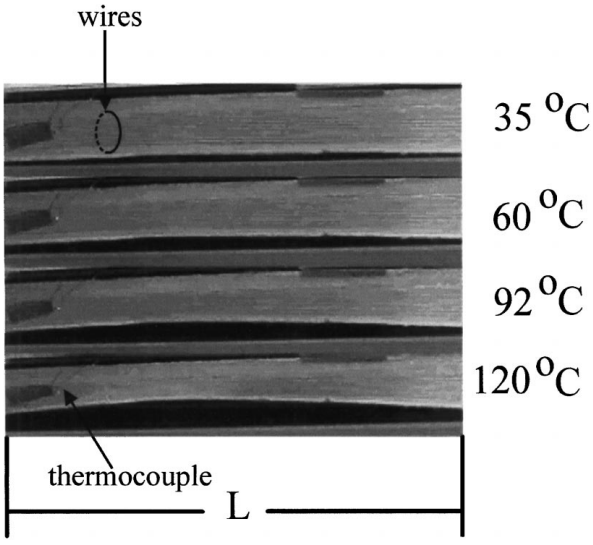

Figure 13 Progressive increase of the amplitude of the buckling deformation for a selected length $L = 50$ mm (Fig. 12) and for four different activation temperatures of 35, 60, 92, 120 °C.

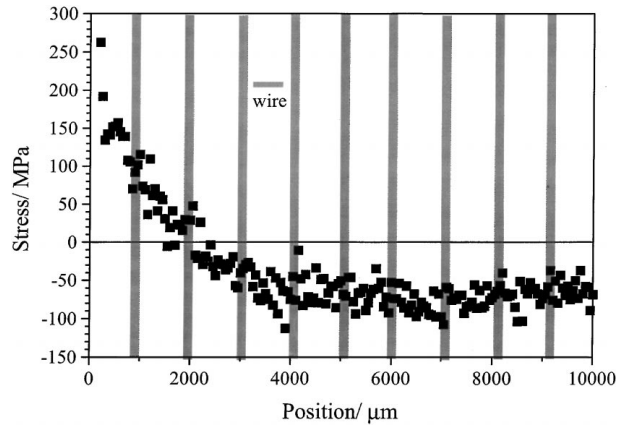

Figure 14 Fibre stresses as measured by the 1611 cm^{-1} Raman band along a 10 mm length of the $O_1^0/W_9/O_1^0$ specimen at ambient temperature. The specimen has been cycled to a high activation temperature of 130 °C (Fig. 12) and exhibits a permanent buckling deformation.

and 6). The Raman wavenumber shift, $\Delta\nu$ scales linearly with either stress, σ, or temperature, θ, and can be expressed by:

$$\Delta\nu_{M,1611} = k_{1611}\sigma \tag{11}$$

$$\Delta\nu_{\theta,1611} = \alpha_{1611}\theta \tag{12}$$

where $\Delta\nu_{M,1611}$ is the wavenumber shift due to mechanical stress (wire transformation), $\Delta\nu_{\theta,1611}$ is the wavenumber shift due to temperature, $k_{1611} = -4.0 \pm 0.4$ cm^{-1}/GPa and $\alpha_{1611} = -0.015 \pm 0.001$ $cm^{-1}/°C$.

By combining (7), (11) and (12) the following expression can be derived for the temperature, θ.

$$\theta = \frac{\Delta\nu_{1611} - \Delta\nu_{R,1611} - k_{1611}\sigma}{\alpha_{1611}} \tag{13}$$

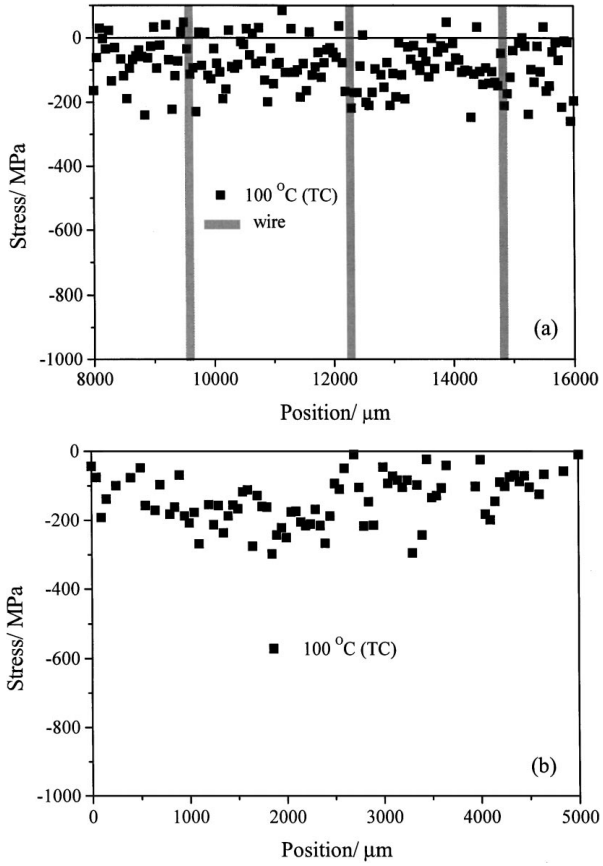

Figure 15 Evaluation of generated stresses due to the 1648 cm^{-1} band for the $O_1^0/W_3/O_1^0$ specimen at 100 °C. (a) Across the wire direction, solid vertical lines represent the SMA wires, and (b) along the wire direction.

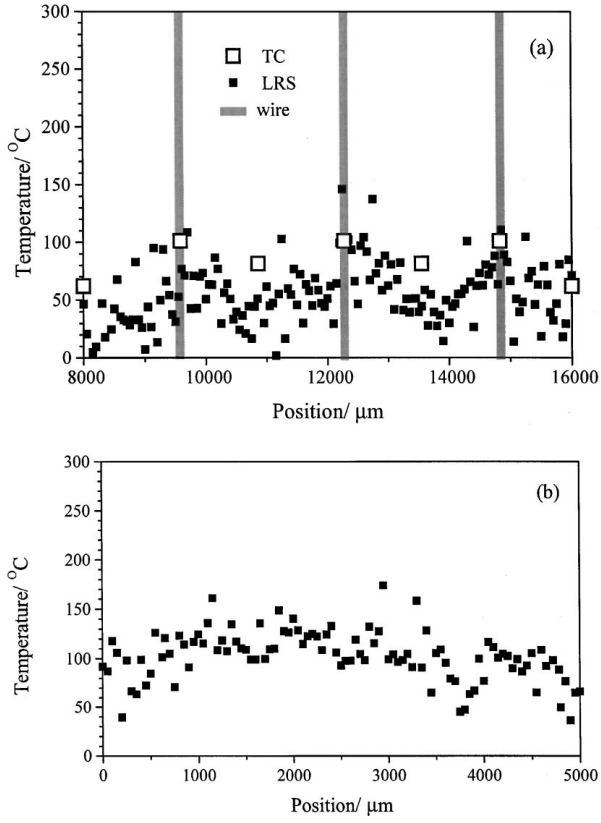

Figure 16 Conversion to temperature due to the 1611 cm^{-1} Raman response of fibres in the $O_1^0/W_3/O_1^0$ specimen. (a) Across the wire direction. The solid vertical lines depict the location of the SMA wires. The values obtained by the thermocouples are also indicated on the graph. (b) Along the wire direction.

where $\Delta\nu_{\theta,1611}$ is the total wavenumber shift. Since the value of σ for each level of actuation (temperature) can be measured independently from Equation 10 then the temperature distribution can be easily obtained from (13).

Temperature distributions calculated by Equation 13, using the point-by-point LRS measurements for the $O_1^0/W_3/O_1^0$ specimen are given in Fig. 16a and b along lines perpendicular and parallel to the wire direction, respectively. The temperature distribution for the perpendicular direction fluctuates from approximately ambient temperature at the mid-wire distance to about 100°C at positions situated just above each wire. Temperature measurements obtained via thermocouples that have been placed at different locations on the specimen surface are also shown in Fig. 16a. As can be seen, there is a very good agreement between the two sets- Raman and thermocouple- measurements. The resulting differences and the scatter of the data points are attributed to (a) different sampling areas (resin surface for the thermocouple vs. embedded aramid fibres for LRS) (b) the experimental error but also (c) real fluctuations of temperature from fibre-to-fibre due to the complex topology of the fibrous specimens. To our knowledge this is the first time that a temperature distribution in fibre reinforced composites is obtained with a spatial resolution of about 1 μm.

The temperature distribution in the direction parallel to the wire length over a distance of 5 mm (Fig. 16b) exhibits a much smaller scatter at any given position but overall it ranges from a lower value of 50°C to a maximum of about 125°C. Again these variations are mainly due to the complexity of the material and the way heat is dissipated rather than the experimental error.

4.2.2. $O_1^0/W_9/O_1^0$ specimen

By increasing the volume fraction of wires the thin 2 ply $O_1^0/W_9/O_1^0$ showed clear signs of geometrical buckling failure even at low values of activation temperature (∼50°C). This is a clear sign that the high stiffness environment of the composite host material results in the generation of high recovery stresses by the pre-strained SMA wires. As shown in Fig. 12, the type of failure reminisces clear plate buckling under compressive load. Such an effect was not observed in the case of the $O_1^0/W_3/O_1^0$ specimen because the generated stress during the experiment was of lower magnitude than the critical load required for geometrical (Euler) plate buckling [26]. In future experiments, an attempt will be made to avoid buckling instabilities by manufacturing short hybrid coupons that do not exhibit geometric buckling for the range of stresses generated by the SMA even at high wire volume fractions.

5. Conclusions

Pre-strained shape memory alloy wires have been inserted by means of a micromechanical device between Kevlar 29/LTM217 epoxy pre-impregnated tapes and

have been cured in an autoclave. The residual thermal stresses that are generated in the aramid fibres as a result of the high temperature curing process were measured in laminates that contained no wires and in hybrid composites of varying wire volume fraction. The results indicated that the presence of the wires reduced the compressive stress that the fibres are subjected to when the laminate is cooled down to ambient temperature. Two adjacent vibrational modes of the aramid Raman spectrum at 1611 and 1648 cm^{-1} were employed for the stress and temperature measurements. The 1611 cm^{-1} band was both stress and temperature sensitive whereas the 1648 cm^{-1} peak was only stress sensitive. A methodology was thus developed whereby the fibre stresses generated in the laminate by wire activation were identified through the 1648 cm^{-1} band while the temperature could then deconvoluted from the shift of the 1611 cm^{-1} band. Generated fibre stresses of average 122 MPa could be measured at the vicinity of the SMA wires whereas the temperature distributions derived by laser Raman yielded similar measurements with those obtained by thermocouples attached on the surface of the specimen. Finally, by increasing the volume fraction of the wires the generated stresses in the laminate were so high that led to plate instability even at low activation temperatures. In the second part of this series of papers, the effect of the SMA volume fraction and laminate geometry upon stress generation will be examined in detail.

Acknowledgements

The reported studies are part of an EU BRITE/EURAM project (No: BRPR-CT97-468). The authors would also like to thank Dr. R. Stalmans and Prof. J. Van Humbeeck of MTM dep. of KU Leuven for supplying the SMA wires. Dr. D. Tunnicliffe and Mrs J. Hudd from BAe Systems for preparing the specimens. Dr. R. Gotthardt and Dr. V. Michaud of Ecole Polytechnique Federale de Lausanne for designing and manufacturing the frame used in the autocalve. Finally we would like to thank all the above for useful suggestions and comments.

References

1. M. F. ASHBY, "Materials Selection in Mechanical Design" (Pergamon Press, 1992).
2. M. V. GANDHI and B. S. THOMPSON, "Smart Materials and Structures" (Chapman & Hall, 1992).
3. L. DELAY, in "Materials Science and Technology, Vol. 5: Phase Transformation in Materials," edited by P. Haasen (VCH Verlagsgesellschaft mbH, Weinheim, Germany, 1991) p. 339.
4. K. OTSUKA and K. SHIMIZU, *International Metals Reviews* **31** (1986) 93.
5. R. STALMANS, in "Advances in Science and Technology, Vol. 25: Smart Materials Systems," edited by P. Vincenzini (Techna, Faenza, Italy, 1999) p. 83.
6. Y. SUZUKI and Y. SEKIGUCHI, in "Shape Memory Alloys," edited by H. Funakubo (Gordon and Breach Science Publishers, Amsterdam, 1987).
7. K. D. JONNALAGADDA, N. R. SOTTOS, M. A. QIDWAI and D. C. LAGOUDAS, *J. of Intell. Mat. Sys. and Struc.* **9**(5) (1998) 379.
8. A. BAZ and J. RO, *Composites Engineering* **2**(5–7) (1992) 527.
9. Z. CHAUDRY and C. ROGERS, in Proceedings of the 32nd Smart Structures and Materials Conference (1991) AIAA-91-1166-CP, p. 186.
10. D. A. HEBDA, M. E. WHITLOCK, J. B. DITMAN and S. R. WHITE, *J. of Intelligent Materials and Smart Systems* **6**(2) (1995) 220.
11. J. S. N. PAINE and C. A. ROGERS, Adaptive Structures and Materials Systems, ASME AD-35, 1993, p. 63.
12. J. E. BIDAUX, L. BATAILLARD, J. A. MANSON and R. GOTTHARDT, in Proceedings of 3rd European Conf. on Advanced Materials and Processes (1993) p. 1.
13. J. S. N. PAINE and C. A. ROGERS, *J. of Thermoplastic Composite Materials* **2**(4) (1991) 102.
14. T. W. DUERING, K. N. MELTON, D. STÖCKEL and C. M. WAYMAN, "Engineering Aspects of Shape Memory Alloys" (Butterworth-Heinemann, London, 1990).
15. J. E. BIDAUX, J. A. E. MANSON and R. GOTTHARDT, *Mat. Res. Soc. Proc.* **459** (1997) 107.
16. C. GALIOTIS, in "Microstructural Characterisation of Fibre-Reinforced Composites," edited by J. Summerscales (Woodhead Pub. Co., 1998).
17. C. GALIOTIS, *Comp. Sci. Technol.* **42** (1991) 125.
18. C. VLATTAS and C. GALIOTIS, *Polymer* **35**(11) (1994) 2335.
19. A. PAIPETIS, C. VLATAS and C. GALIOTIS, *Journal of Raman Spectroscopy* **27** (1996) 519.
20. P. K. KIM, C. CHANG and S. L. HSU, *Polymer* **27** (1986) 34.
21. C. FILIOU, C. GALIOTIS and D. N. BATHELDER, *Composites* **23**(1) (1991) 28.
22. C. FILIOU and C. GALIOTIS, *Comp. Sci. and Tech.* **59/14** (1999) 2149.
23. C. F. DIETRICH, "Uncertainty, Calibration, Probability," The Adam Hilger Series on Measurements Science and Technology, 2nd ed. (Bristol, 1991).
24. J. A. NAIRN and P. ZOLLER, *J. Mater. Sci.* **20** (1985) 355.
25. G. C. PSARRAS, J. PARTHENIOS and C. GALIOTIS, in ECCM9 Conference, Brighton, U.K., 4–7 June 2000.
26. S. P. TIMOSHENKO and J. M. GERE, "Theory of Elastic Stability" (McGraw Hill Co, 1963).

Received 10 April
and accepted 27 June 2000